Dalton Transactions

Accepted Manuscript

ROYAL SOCIETY OF CHEMISTRY

www.rsc.org/dalton

Journal Name

RSCPublishing

ARTICLE

Cobalt Complexes of Tetradentate, Bipyridine-Based Macrocycles; their Structures, Properties and Photocatalytic Proton Reduction

Cite this: DOI: 10.1039/x0xx00000x

Received 05th Febuary 2015,
Accepted 00th January 2012

DOI: 10.1039/x0xx00000x

www.rsc.org/

E. Joliat,[a,c] S. Schnidrig,[a,c] B. Probst,[a] C. Bachmann,[a] B. Spingler,[a] K. K Baldridge,[a] F. von Rohr,[b] A. Schilling[b] and R. Alberto*[a]

Complexes with purely pyridine-based macrocycles are rarely studied in photo(electro)catalysis. We synthesized and investigated macrocycles, in which two 2,2'-bipyridine (bpy) units are linked twice by two cyano-methylene groups, to yield the basic tetradentate, bipyridine based ligand framework (pyr). The protons in the bridges were substituted to obtain derivatives with one (pyr-alk) or two (pyr-alk$_2$) alkyl-chains, respectively. We present the crystal structures of the *mono*-pentylated and the *cis*-dibutylated ligands. The corresponding Co^{II} complexes [$Co^{II}(OH_2)_2$(pyr)], [Co^{II}Br(HOMe)(pyr-bu)], [$Co^{II}Br_2$(*cis*-pyr-bu$_2$)] and [$Co^{II}Br_2$(*trans*-pyr-bu$_2$)] were prepared, their physico-chemical properties elucidated and their crystal structures determined. X-ray analyses revealed for the latter three complexes distorted octahedral coordination and a fairly planar {Co^{II}(pyr)} macrocyclic scaffold. The axial bromides in [Co^{II}Br(HOMe)(pyr-bu)], [$Co^{II}Br_2$(*cis*-pyr-bu$_2$)] and [$Co^{II}Br_2$(*trans*-pyr-bu$_2$)] are weakly bound and dissociate upon dissolution in water. While the alkylated complexes are paramagnetic and feature Co^{II} d^7 high spin configurations, the unsubstituted complex [$Co^{II}(OH_2)_2$(pyr)] displays a rare Co^{II} low spin configuration. The electronic ground states of [$Co^{II}Br_2$(*cis*-pyr-bu$_2$)] and [$Co^{II}Br_2$(*trans*-pyr-bu$_2$)] are similar, as evident from the almost identical UV/vis spectra. Electrochemical analyses show redox-non-innocent ligand frameworks. All complexes are highly robust and efficient H^+ reducing catalysts. In the presence of [Ru(bpy)$_3$]Cl$_2$ as photosensitizer and TCEP/NaHasc as sacrificial electron donor and shuttle, turnover numbers (TONs, H_2/Co) up to 22'000 were achieved.

Introduction

Sunlight is the most promising source of renewable energy: Within one hour the sun provides with a power of 120'000 terawatt as much energy as mankind needs in one year.[1] Moreover, unlike fossil fuels it is a carbon-free energy source, available in any region of the world, and in contrast to other sources of power, hazard-free. An elegant way to store harvested sunlight is the conversion of solar energy into chemical energy. Photocatalytic water splitting follows exactly this principle: Catalysts and photosensitizers split water into its elements to produce H_2 as a clean source of energy and O_2. In this way, solar energy is stored in the chemical bonds of H_2 and O_2. Using H_2 as a fuel releases H_2O as the only product of combustion – the renewable cycle is closed. Photocatalytic water splitting represents therefore an environmentally friendly way to unlimited fuel supply. Due to its complexity, the overall process is divided in a reductive and an oxidative part and each half reaction is usually studied separately. Water reduction catalysts (WRCs) based on non-precious metals are typically complexes containing iron,[2] cobalt,[3-6] nickel[7] and molybdenum[8] as central atoms, among which cobalt and nickel are the most active metal centers. Co complexes with glyoximato or tetraimine type ligands were amongst the first WRCs for homogeneous, photocatalytic water reduction.[3] As catalysis was often terminated due to WRC decomposition, much effort was put in the development of more robust complexes. Acyclic polypyridyl cobalt complexes emerged as a class of efficient WRCs.[9-11] We reported recently Co^{II} complexes with tetra-[12] and pentapyridyl[13] ligands, which are highly active catalysts in aqueous photocatalytic H_2 production. Macrocycles, however, can provide even higher binding affinity towards metal ions and porphyrin complexes, used in numerous fields of chemical science and in nature, are probably the prototypes, consisting solely of heterocyclic building blocks (tetra-pyrroles). Few studies have been reported with cobalt complexes of porphyrins in the context of photocatalysis. So far, long-term stabilities and efficiencies are not encouraging enough for pursuing studies with these catalysts or ligands respectively.[14, 15] An alternative to pyrrole-based macrocycles are ring-systems comprising four pyridines as donors. This kind of macrocycles resembles porphyrins but consists of *pyr*idine instead of pyrrole units, thus we will abbreviate them as *pyr*phyrins. Pyrphyrins are far

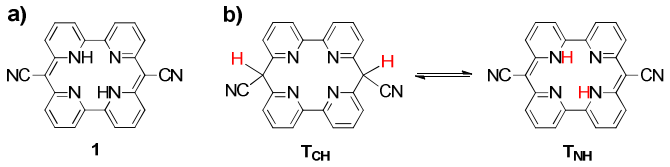

Scheme 1 a) Basic ligand framework of a tetradentate macrocyclic bis-bipyridyl[18] (pyrphyrin). b) Tautomeric forms of pyrphyrins.

less exploited and, to the best of our knowledge, have not been applied to photocatalysis. Among the very few reports involving pyrphyrins or aza-bridged analogues, are studies by *Costamagna et al.* exploring corresponding Co^{II}, Ni^{II} and Cu^{II} complexes for the electrocatalytic reduction of CO_2.[16,17] The basic pyrphyrin ligand framework (**1**, Scheme 1a) was introduced by *Ogawa* and coworkers as early as 1984.[18] This framework served as the starting point for several derivatives, such as alkylated[19-21] or decyanated[18] pyrphyrins as well as various pyrphyrin metal complexes.[19,22,23] A particularly interesting property of pyrphyrins or their aza-bridged analogues is the tautomerism between a formally doubly condensate bpy and a fully conjugated macrocycle (Scheme 1b).[18,24-26] The success of acyclic polypyridyl of Co^{II} in proton reduction was our incentive to study their cyclic tetradentate congeners[27-31] and to investigate their properties and applications. In this work, syntheses, characterization and performance of Co^{II} pyrphyrin complexes in aqueous photocatalysis are presented.

Results and discussion

Synthesis of the ligands: The starting compound for all subsequent derivatizations is the pyrphyrin (pyr) ligand (**1**) shown in Scheme 1. This compound was synthesized along a modified procedure reported by *Ogawa* and coworkers[18] and purified by vacuum sublimation at 350 °C and 10^{-5} mbar. Compound **1** is essentially insoluble in all solvents, likely due to its planar structure resulting in strong stacking interactions. The protons are therefore localized on the pyridine nitrogens with two 2-pyridyl-2(1H)-pyridylideneacetonitrile bridges as illustrated in the right structure ($\mathbf{T_{NH}}$) in Scheme 1b. B97D/Def2-TZVPP (DMF) calculated structures also predict a significant stability associated with tautomer $\mathbf{T_{NH}}$ compared to $\mathbf{T_{CH}}$ (30.4 kcal/mol for the *cis*-$\mathbf{T_{CH}}$ and 28.6 kcal/mol for the *trans*-$\mathbf{T_{CH}}$ form with respect to planar $\mathbf{T_{NH}}$ form). To enhance the solubility and to introduce functional groups at the cyano-methylene bridge, we coupled alkyl-chains to **1**. Reaction with 1-iodo-butane resulted in a mixture of *mono*-butyl-pyrphyrin (pyr-bu, **2**), *cis*- and *trans*-dibutyl-pyrphyrin (*cis*-pyr-bu_2, **3** and *trans*-pyr-bu_2, **4**, Scheme 2)[19] which could be separated by a new column chromatography method on silica (ESI). With alkyl-bromide instead of alkyl-iodide (e.g. 1-bromo-pentane or -butane), di-alkylation was suppressed and only the *mono*-alkylated product was obtained. In the original procedure, large excess of NaH (base, ca. 20 eq.) and alkylating agent (ca. 35 eq.) were used, which made workup rather unpredictable. Close to stoichiometric amounts of KO^{t}Bu and 1-iodo-butane yielded exclusive formation of *mono*-butyl-pyrphyrin (**2**) in approximately 30 % yield after purification. The alkylated compounds **2–4** are well soluble in organic solvents. Stacking interactions are reduced and the lower symmetry of the ligands should lead to an increased dipole moment, favorable for solubility. Single crystals of **3** could be obtained by vapor diffusion[32] of cyclopentane into a saturated solution of **3** in CH_2Cl_2. Since **2** did not give suitable single crystals for X-ray analysis, we synthesized the corresponding pentyl derivative (*mono*-pentyl-pyrphyrin, **5**), for which single crystals were obtained.

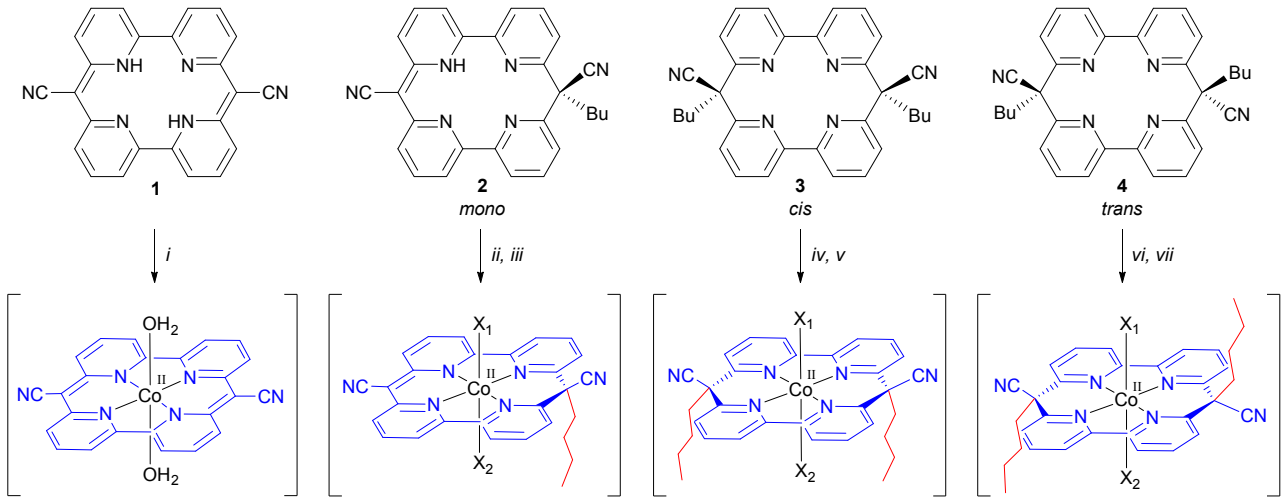

Scheme 2 Preparation of cobalt complexes with ligands **1**–**4**. Highlighted in blue: pyrphyrin scaffold. i) $Co(OAc)_2$ tetrahydrate, KO^{t}Bu, pyridine reflux, 2 h, 89 %; *ii*) $CoBr_2$ hydrate, NaOH, MeOH, reflux, 2 d, 83 %; *iii*) $Co(ClO_4)_2$ hexahydrate, NaOH, MeOH, reflux, 4 d, 53 %; *iv*) $CoBr_2$ hydrate, EtOH, reflux, 2 h, 66 %; *v*) $Co(ClO_4)_2$ hexahydrate, CH_3CN, 25 °C to reflux, 23 h, 69 %; *vi*) $CoBr_2$, EtOH, reflux, 2 h, 63 %; vii) $Co(ClO_4)_2$ hexahydrate, CH_3CN, 25 °C to reflux, 45 h, 71 %.

Journal Name RSCPublishing

ARTICLE

Crystal structures of the ligands: According to B97D/Def2-TZVPP (DMF) calculations, the structure **1** in gas phase is fully planar. The solution phase structure has a very slight out of plane twist in the pyridyl components but is fully planar around the –C-CN units. The two cyano-substituents are aligned in an anti-parallel fashion (Figure 1a). This planarity is strongly disturbed upon formation of **2**. The B97D/Def2-TZVPP (DMF) calculated structure of **2** and the X-ray structure of **5** are shown in Figure 1b-c. The geometry of **5** has a planar 2-pyridyl-2(1*H*)-pyridylideneacetonitrile moiety and a non-planar pentyl di(2-pyridyl)acetonitrile moiety (Figure 1c). The cyano-groups are still aligned in an anti-parallel orientation, occupying the equatorial position relative to the macrocycle. The orientation of the pentyl group is uncommon since it stands almost perpendicular to the plane formed by the four nitrogen atoms. The assignment of the N3-H proton position is supported by additional electron-density next to N3 as well as the longer C–N bond lengths of this "dearomatized" pyridine (1.365(3) (N3–C12) and 1.377(2) Å (N3–C16)) compared with the pyridine on the pentyl di(2-pyridyl)acetonitrile moiety (1.329(3)–1.345(2) Å).

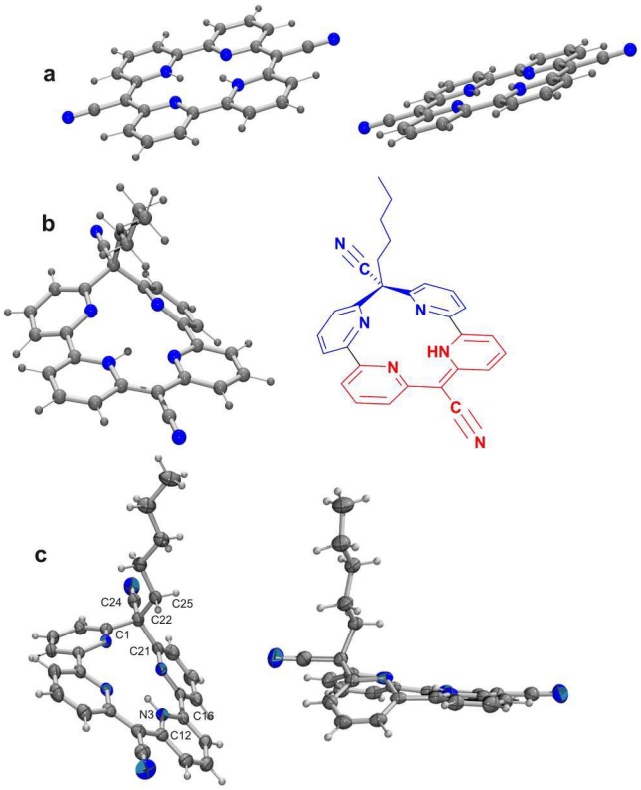

Fig. 1 a) B97D/Def2-TZVPP (DMF) calculated structure of **1** and b) of **2** and schematic representation of the planar (red) and non-planar (blue) moiety within the macrocycle pyr-pent (**5**). c) Top and side views ORTEP[33] of **5**. Thermal ellipsoids are at the 50 % probability level.

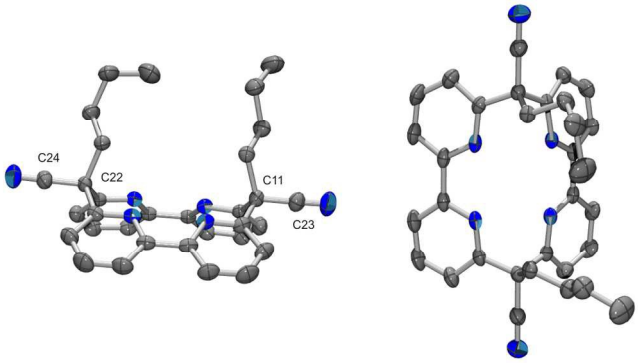

Fig. 2 ORTEP of *cis*-pyr-bu$_2$ (**3**), side and top view. Ellipsoids are drawn at the 50 % probability level. Only one out of two molecules in the asymmetric unit is displayed, hydrogen atoms are omitted for clarity.

Upon introduction of a second alkyl substituent, the geometry changes considerably and the basic pyrphyrin framework adopts a book shape conformation. The structures of *cis*-pyr-bu$_2$ (**3**) was determined by X-ray structure analyses and B97D/Def2-TZVPP (DMF) calculations (Figure 2 and S1). Both, experimental and calculated structures reveal the folded shape, with the *cis*-configuration of the alkyl substituents predicted to be more stable than the *trans*-form by 6.7 kcal/mol. Indeed, syntheses always yielded a higher amount of **3** than of its diastereomer **4**, in agreement with the theoretical prediction. Due to rehybridization of the bridging carbons between the two bpy moieties from sp^2 to sp^3 upon alkylation of **1**, the two bpy units fold towards each other. In analogy to structure **2**, both alkyl groups in **3** are approximately perpendicular with respect to the plane formed by the four nitrogen atoms. The structure of diastereomer **4** was reported by *Ogawa* et al.,[19] showing two strongly twisted pyridine units within the bpy moieties. The cyano groups are still essentially linearly oriented. Due to the interruption of conjugation, compounds **3** and **4** are almost colorless.

Synthesis of the cobalt complexes: Complexes **1a**–**4a** were prepared by reaction of the respective ligands with $CoBr_2$, $Co(OAc)_2$ or $Co(ClO_4)_2$ in refluxing pyridine, CH_3CN, EtOH or MeOH (Scheme 2). [Co^{II}(pyr)$(OH_2)_2$] **1a**, [Co^{II}Br(HOMe)(pyr-bu)] **2a**, [$Co^{II}Br_2$(*cis*-pyr-bu$_2$)] **3a** and [$Co^{II}Br_2$(*trans*-pyr-bu$_2$)] **4a** as well as their bromide-free analogues [Co^{II}(THF)(pyr-bu)][ClO_4] **2b**, [$Co^{II}(OH_2)_2$(*cis*-pyr-bu$_2$)][ClO_4]$_2$ **3b** and [$Co^{II}(OH_2)_2$(*trans*-pyr-bu$_2$)][ClO_4]$_2$ **4b** were obtained in good yields (see ESI). HR-ESI-MS data are in support of the respective compositions with the following experimental vs. calculated m/z data; **1a**; 443.0445 [M – 2 H_2O]$^+$, vs. [$C_{24}H_{12}CoN_6$]$^+$ 443.0450), **2a**; 500.1160 [M – Br – CH_3OH]$^+$ vs. [$C_{28}H_{21}CoN_6$]$^+$ 500.1154), **3a**; 636.1043 [M – Br]$^+$ vs. [$C_{32}H_{30}BrCoN_6$]$^+$ 636.1042 and **4a**; 636.1052 [M – Br]$^+$ vs.

$[C_{32}H_{30}BrCoN_6]^+$ 636.1042. The bromide-free analogues gave **2b**; 500.1155 $[M - ClO_4 - THF]^+$, vs. $[C_{28}H_{21}CoN_6]^+$ 500.1154), **3b**; 278.5930 $[M - 2\ H_2O]^{2+}$, vs. $[C_{32}H_{30}CoN_6]^{2+}$ 278.5927 and **4b**; 278.5927, $[M - 2\ H_2O]^{2+}$, vs. $[C_{32}H_{30}CoN_6]^{2+}$ 278.5927. Deprotonation of the ligands **1** and **2** with KO^{t}Bu or NaOH was required for efficient complexation. Purification was achieved by trituration for **1a** or washing with water for **2a** and **2b**. In solid form, all three complexes are nearly black in color. Recrystallization from EtOH and MeOH yielded **3a** and **4a** in high purities as dark red solids. While **1a** is only soluble in pyridine, **2a**–**4a** are well soluble in most solvents, including water. The assumed stronger permanent molecular dipole moment in **3a** may be responsible for its higher solubility in polar solvents as compared to its diastereomer **4a**.

Crystal structures of the Co^{II} complexes reveal for all three Co^{II} bromo-complexes **2a**–**4a** a *Jahn-Teller* distorted octahedral geometry (Figure 3). The four pyridine nitrogens are in the equatorial plane and the axial bromides (or a methanol in **2a**) occupy the axial positions. Complex **4a** is centrosymmetric. The Co–Br distances are (Co1–Br1) 2.8231(10) Å in **2a**, (Co1–Br1) 2.6791(4) Å and (Co1–Br2) 2.8386(4) Å in **3a**, and (Co1–Br1) 2.7741(2) Å in **4a**. These very long bonds almost reach the sum of the *van der Waals* radii of bromide and cobalt (2.9 Å)[34] and are the second longest reported to date.[35] The twisted or book-shaped (vide supra) bpy moieties in the free ligands become nearly co-planar in the corresponding Co^{II} complexes. As for the ligands **2** and **3**, the butyl chains in **2a**–**4a** are about perpendicular to the pyr plane, whereas the nitriles are parallel to it. Remarkably, we did not find any experimental evidence for the existence of corresponding diastereomers, i.e. structures with the nitriles oriented out of the macrocyclic plane. The observed configurations allow for partial electronic interaction, i.e. negative hyperconjugation or anomeric effect between the nitrile groups and the macrocyclic ring, in line with calculations (ESI, Figures S2-3). The crystal structures coincide with this hypothesis; the bond lengths of C22–C25 (complexes **2a** and **3a**) and C11–C12 (complex **4a**), respectively, are in the range between 1.567(2) and 1.577(2) Å, and thus significantly longer than a common single bond between two sp^3 hybridized carbon atoms (1.53 Å).[36] The sum of the three angles between the pyridyl units and the nitrile group, centered at the bridging carbons, range between 327.9(5)° and 330.17(28)° for the ligands **3** and **5** but are substantially widened to 334.26(25)° and 336.87(24)° for the three complexes **2a**–**4a**. Upon metallation, the bpy units become almost coplanar relative to each other. In the free ligands, the dihedral angles between the bpy planes are 35.97(6)° for **5** and 66.50(9)° or 67.98(9)° for **3**. Upon coordination to Co^{II}, they flatten down to 18.38(15)° and 15.44(5) for **2a** and **3a**, respectively. The bridging, formally sp^3-hybridized carbon atoms C22 and C11 interrupt the surrounding sp^2 hybridized carbons of the bpy systems and the nitrile moiety. The in parallel aligned nitrile moieties, however, favor conjugation with the pyrphyrin scaffold. To minimize electronic constraints, the bridging carbon atoms adopt partial sp^2 character, thereby allowing for electronic communication over the whole ligand framework. The presence of π-electron density at C22 and C11 finally leads to negative hyperconjugation: Electron density is pushed into the σ* orbital of the C22–C25 (**2a** and **3a**) and C11–C22 (**4a**) carbons bonds, thereby weakening and elongating these bonds as indicated in the crystal structures and confirmed by calculations. Thus, we interpret these structural changes upon metallation as an anomeric effect, resp. negative hyperconjugation.

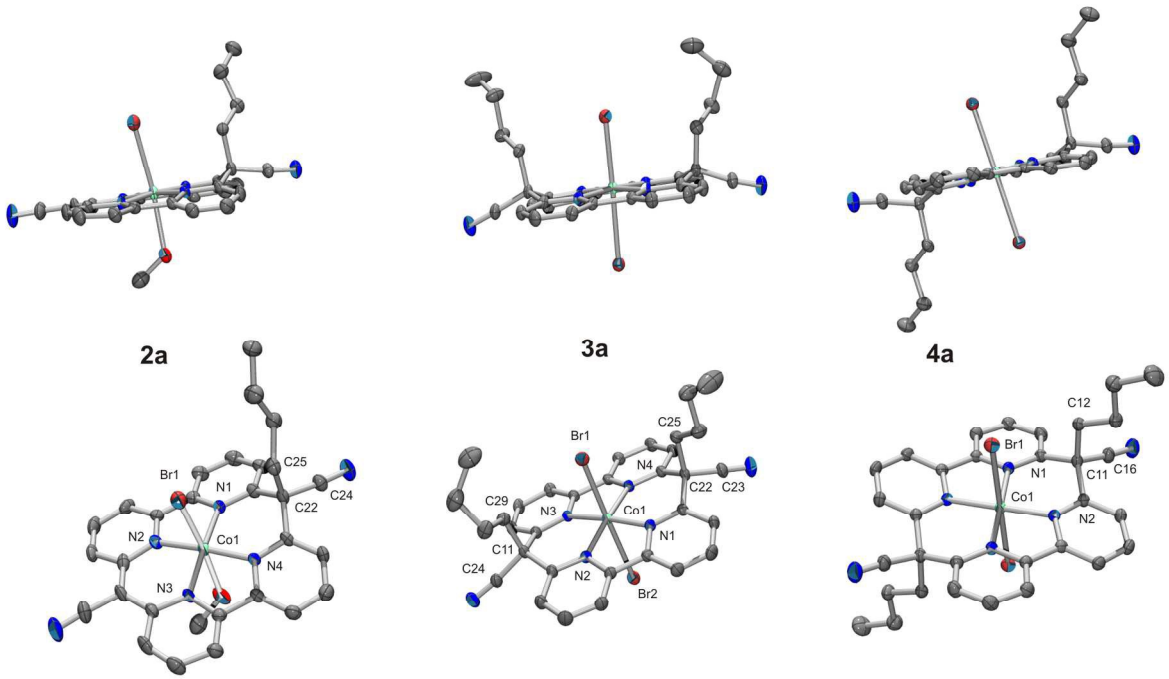

Fig. 3 ORTEP representation of **2a**, **3a** and **4a** with selected labels. Thermal ellipsoids are at the 50 % probability level, hydrogen atoms and solvent molecules omitted for clarity. Selected bond lengths [Å] and angles [°]: **2a**: Co1–Br1 2.8231(10), Co1–N1 1.925(4), Co1–N2 1.904(4), Co1–N3 1.897(4), Co1–N4 1.922(4), C22–C24 1.478(8), C22–C25 1.569(7); **3a**: Co1–Br1 2.6791(4), Co1–Br2 2.8386(4), Co1–N1 1.9220(14), Co1–N2 1.9290(14), Co1–N3 1.9219(14), Co1–N4

1.9278(14), C22–C23 1.483(3), C22–C25 1.572(3), C11–C24 1.485(2), C11–C29 1.567(2); **4a**: Co1–Br1 2.7741(2), Co1–N1 1.9250(13), Co1–N2 1.9248(13), C11–C16 1.484(2), C11–C12 1.577(2).

SQUID magnetometry: The absence of resonances in the ^{1}H NMR spectra of **1a**–**4a** agrees with paramagnetic Co^{II} centers and entails the question about their spin states. Generally, high spin states for such d^7 systems are assumed but determinations of magnetic susceptibilities are rare. We therefore performed SQUID magnetometry and the magnetic data of **1a**–**4a** could well be explained by the *Curie-Weiss* law. The effective magnetic moments of the complexes **3a** (4.61 μ_B/Co) and **4a** (4.42 μ_B/Co) are larger than the theoretically expected value of 3.87 μ_B/Co for the spin-only magnetic moment of a mononuclear d^7 high spin complex with S = 3/2 Co^{II}. They are, however, in good agreement with the values of other d^7 high spin Co^{II} complexes.[9, 37-40] The magnetic moment of **2a** is 3.52 μ_B/Co and can be correlated to its *Curie*-temperature $\theta \approx$ -3.48 K. This indicates a non-negligible antiferromagnetic interaction between the magnetic centers, for instance π-π stacking leading to a shielding of the external magnetic field and to the overall observed magnetization of **2a** (Figure 4). The measured effective magnetic moment of **1a** is 1.85 μ_B/Co and the lowest in this series. This value corresponds to a low-spin Co^{II} complex.[41, 42] The high *Curie*-temperature ($\theta \approx$ -3.93 K) as well as deviation from the *Curie-Weiss* behavior at low temperatures, are indications for non-trivial electron-electron interactions in **1a**. Our magnetization measurements therefore confirm that complexes **2a**–**4a** (ESI, Figure S4) are Co^{II} complexes with d^7 high spin configuration, while **1a** is a rare example of a low-spin Co^{II} complex (Table 1). The effective magnetic moments are found to decrease with increasing conjugation and π-π stacking within **1a**–**4a**.

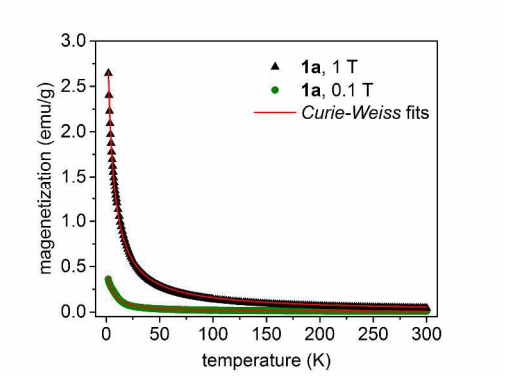

Fig. 4. SQUID magnetometry for **1a** over a temperature range of 300 K at magnetic fields of 0.1 and 1.0 T and corresponding *Curie-Weiss* fit.

Table 1. Summary of magnetic properties of complexes **1a**–**4a**: *Curie*-temperatures T_C (Θ) and effective magnetic moments μ_{eff} per cobalt center.

Compound	Θ (K)	μ_{eff} (μ_B)
1a	-3.93	1.85
2a	-3.48	3.52
3a	-0.25	4.61
4a	-0.28	4.42

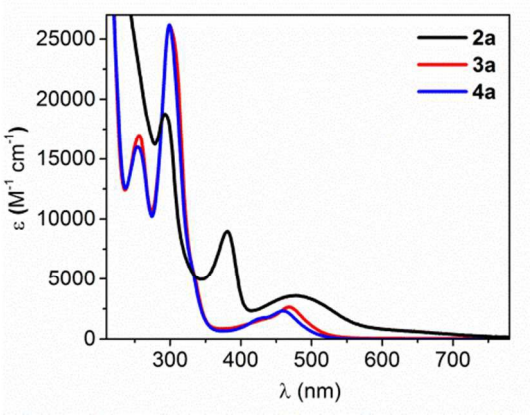

Fig. 5 UV/vis spectra of **2a**, **3a** and **4a** in water.

IR and UV/vis spectroscopy: Wavenumbers and band intensities of C≡N valence vibration modes are indicative for their electronic environment. Literature predicts weak bands for aliphatic nitriles between 2260 and 2200 cm^{-1} and stronger, red-shifted bands in conjugated systems.[43] Our ligands and complexes follow these general trends. The vibrations of the conjugated nitriles in the free macrocyles **1** and **2** are very intense (both 2181 cm^{-1}) whereas weak bands are found for **3** and **4** at 2241 (calc. 2249) and 2244 (calc. 2252) cm^{-1}. The nitrile bands shift to lower energies upon complexation by cobalt, giving strong bands at 2165 for **1a** and 2171 cm^{-1} (conjugated CN) for **2a**, respectively (for comparison, B97D/Def2-TZVPP gives **2a** at 2168 cm^{-1}). The nitrile bands of the alkyl-di(2-pyridyl)acetonitrile units are extremely weak, and could not unambiguously be identified in **2** or **2a**.

The UV/vis spectra of [Co^{II}Br(HOMe)(pyr-bu)] (**2a**, Figure 5) and the free ligand **2** are very similar. A broad absorbance in the visible range (480 nm) is indicative for a planar macrocyclic ligand framework. Since absent in the dibutylated complexes **3a** and **4a**, a distinct band at 381 nm is assigned to the 2-pyridyl-2(1H)-pyridylideneacetonitrile unit. A strong band at 293 nm and a shoulder at 250 nm complete the spectra. Based on the comparison with the spectrum of the free ligand, we assign the additional absorption at 650 nm (weak shoulder) to a cobalt-based transition. Our assignments are in coincidence with calculated ones for the almost identical spectrum of the Zn^{II} complex of ligand **2**.[22] The UV/vis spectra of complexes **3a** and **4a** in water are very similar (Figure 5). The characteristic 2,2'-bipyridine absorptions at 299 nm increases in intensity and indicate two electronically weakly coupled, planar 2,2'-bipyridine units, also observed in the free ligand.[19] The weak absorptions ($\varepsilon \approx$ 2'500 M^{-1}cm^{-1}) at 450 nm are absent in the case of the bent, free ligands. As indicated by calculations, we assign these bands to cobalt-based transitions.

Bromide dissociation in water was observed for all water-soluble complexes. Upon dissolution of the bromide complexes **2a**–**4a** in

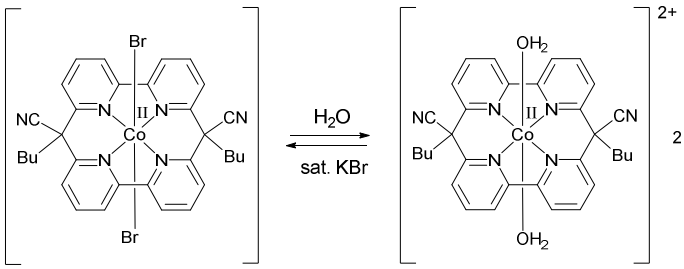

3a / 4a — dark wine red solid

[3b]$^{2+}$ / [4b]$^{2+}$ — yellow solution

Scheme 3 Equilibrium of Br^- dissociation in water for complexes **3a**, **3b**, **4a** and **4b**.

water, the same UV/vis spectra as those of the bromide-free analogues **2b**–**4b** were obtained (ESI, Figure S5). Of note,dissolution of dark wine red solids **3a** or **4a** gave yellow solutions of **3b** and **4b** respectively. Addition of up to 14 eq. KBr did not change the UV/vis absorption (ESI, Figure S6), indicating a weak Br^- association constant. However, adding a saturated KBr solution lead again to dark wine red crystals after standing over night of e.g. **3a**, supporting reversible exchange of Br^- by water to yield the dication $[Co^{II}(OH_2)_2(cis/trans\text{-pyr-bu}_2)]^{2+}$ (Scheme 3).

Electrochemistry: Cyclovoltametry of the cobalt complexes of ligand **2** exhibited two reductions, whereas three or more were observed for complexes of **3** and **4** in DMF up to -2 V vs $Fc^{0/+}$ (Table 2). Based on the comparison with the protonated ligands **2**–**4**, the second, reversible reduction is assigned to a ligand based process (-1.8 V for **2a**, -1.3 V for **3a** and **4a**, all vs. $Fc^{0/+}$). The first, reversible reductions at -1.1 V for **2a** and -1.0 V for **3a** and **4a** (vs. $Fc^{0/+}$), respectively, are tentatively assigned to a $Co^{II/I}$ process. Only one ligand-based reduction is seen for **2a** with an extended π system, whereas at least two reductions are observed for **3a** and **4a** with interrupted electronic communication between the two bpy units. These assignments parallel the electron donating properties of formally anionic, *mono*-butylated **2** as compared to the neutral, dibutylated ligands **3** and **4**. Since no negative charge is localized on the latter ligands, reduction of their cobalt complexes is facilitated. One reversible oxidative wave was observed at -0.26, -0.14 and -0.11 V vs. $Fc^{0/+}$ for **2a**–**4a**, respectively, in agreement with the electron donating properties of the bromide ligands. Consequently, the oxidation of solvated **2b**–**4b** showed a strong anodic shift (0.19 V for **2a**, and >0.75 V for **3b** and **4b**, vs. $Fc^{0/+}$). The $Co^{II/I}$ potentials are also anodically shifted in the solvated compounds **3b** and **4b** as compared to **3a** and **4a** by about 60 mV, whereas the ligand based reductions display little sensitivity to the axial ligands. It is noteworthy that the potential of reduced PS $[Ru(bpy)_3]^{2+}$ is sufficiently negative to reduce Co^{II} to Co^{I} for all complexes, and also for the first ligand centered reductions in the case of **3b** and **4b**. Electrochemistry at a HMD electrode in water with **2a** and **3a** from pH 2–12 showed catalytic proton reduction at a constant overpotential of 0.79 and 0.77 V, respectively (ESI Figure S7). A slope of 59 and 57 mV per pH unit supports a proton coupled electron transfer in the rate limiting step of catalysis. Due to surface grafting of the once reduced compounds, reductions in H_2O were in all cases irreversible. Whereas reduction of

Table 2. Electrochemical data of the (protonated) ligands **2**–**4**, the respective cobalt complexes and $[Ru(bpy)_3]^{2+}$ (all 1 mM) in DMF and 0.1 M $[^nBu_4N][PF_6]$ as electrolyte in V vs. $Fc^{0/+}$ (GC WE, Pt CE, Ag/AgCl RE).

Compound	$E_M^{III/II}$	$E_M^{II/I}$	E_{L/L^-}	$E_{L^-/L^{2-}}$
2 + 1eq. TFA			-1.91[a]	
2a	-0.26	-1.12	-1.82	
2b	0.19[a]	-1.15	-1.85	
3 + 1eq. TFA			-1.29[a]	
3a	-0.14	-0.97	-1.33	-1.76
3b	–[b]	-0.91	-1.32	-1.74
4 + 1eq. TFA			-1.30[a]	
4a	-0.11	-1.01	-1.33	–[c]
4b	–[b]	-0.95	-1.32	–[c]
$[Ru(bpy)_3]^{2+}$	0.81	-	-1.74	-1.91

[a] irreversible wave, E_{pa} or E_{pc}, respectively; [b] >0.75 V vs $Fc^{0/+}$; [c] several, irreversible peaks.

2a in H_2O is strongly pH dependent over the investigated pH range (ESI, Figure S8), two well-resolved reduction bands are seen for **3a** (ESI, Figure S9). The first peak (FWHM ≈ 90 mV, ESI, Figure S10) corresponds to a one electron reduction[44] at a constant potential up to pH 10 (-0.44 V vs SHE). Above, it shifted more negative, evidencing a characteristic proton coupled electron transfer (PCET). We thus assign this peak to the $Co^{II/I}$ redox couple, consistent with the relative assignment in DMF. The PCET at pH > 10 likely indicates a pK_a of an axial aquo ligand of ~10. The second peak, remains constant at ~-0.54 V vs SHE over the full pH range, and its FWHM (~50 mV) indicates a two electron process,[44] as proposed in DMF for the ligand based reduction.

Photostability: Long-term stability of photocatalysts is crucial for application. Even though the conjugated structures of the cobalt complexes were designed to increase stability as water reduction catalysts, it may make them prone to photolytic decomposition. To assess the respective behaviour, aqueous solutions of **2a**–**4a** were kept in the dark (blank experiments, Ar or air) or under irradiation in an argon atmosphere. HPLC and UV/vis spectra, recorded over a period of 21 days, showed only minor changes for **2a** and **3a** in dilute aqueous solution at µM concentrations in the dark and under light irradiation (ESI, Figures S11–S13). Under the same conditions, **4a** showed distinct UV/vis changes even in the dark, with an emerging band at 380 nm (Figure 6) as observed in **2a**, indicative for the formation of a 2-pyridyl-2(1H)-pyridylideneacetonitrile unit (Figure 4). HPLC analysis showed formation of a new complex and ESI-MS indeed confirmed loss of one butyl substituent from **4a**.

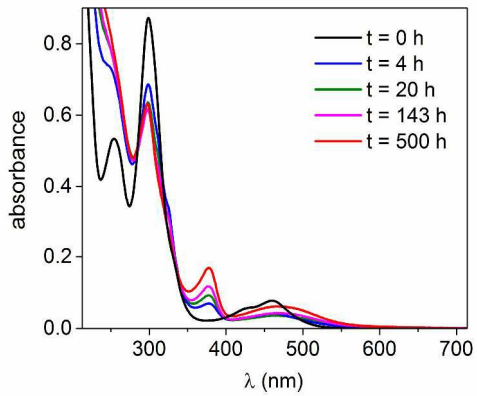

Fig. 6 UV/vis spectra of **4a** (33 μM) in water recorded during 21 d in the dark under an argon atmosphere.

The elongated bond between the bridging carbon and the alkyl chain (C11–C12, Figure 3) rationalizes a facile bond break. **3a**, the *cis*-diastereomer of **4a**, does not show this instability. The crystal structures of ligands **3** and **4** or complexes **3a** and **4a** (Figure 3) reveal a twisted bipyridine conformation in the *trans*-pyr-bu$_2$ systems but a book-like conformation in *cis*-pyr-bu$_2$. They therefore experience different strains and the four pyridyl units in **4** must more strongly rearrange to adopt a planar geometry for coordination. The resulting strain within the macrocycle might partially be released by the loss of one butyl residue, thus generating a 2-pyridyl-2(1*H*)-pyridylideneacetonitrile moiety as present in **2a**.

Photocatalysis: Catalysis with **2a**–**4a** was performed at various WRC concentrations in aqueous solution (10 mL), with ascorbic acid H$_2$asc/[Hasc]$^-$ as sacrificial electron donor (SED) at pH = 5.0 and 0.5 mM $[Ru(bpy)_3]^{2+}$ as photosensitizer (453 nm LED, 0.30 ± 0.02 μE/s). TCEP (tris(2-carboxyethyl)phosphine hydrochloride was added (0.1 M) to recycle oxidized ascorbate (dehydroascorbate DHA).[45] A detailed description, along with a scheme of the experimental setup is shown in the supporting information (ESI, Materials and Methods and Scheme S1).

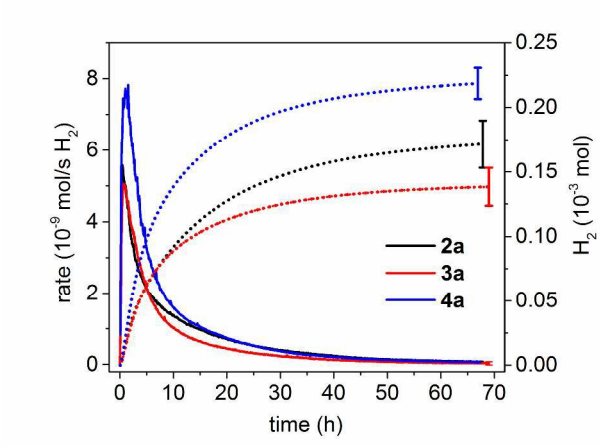

Fig. 7 Hydrogen evolution experiments for solutions of 1 μM catalyst **2a**, **3a** and **4a**, 500 μM $[Ru(bpy)_3]Cl_2$, 0.1 M TCEP, 0.1 M NaHasc, pH 5, 453 nm LED, photon flux of 0.30 ± 0.02 μE/s, V_{tot}=10 mL. Solid line: rate of H$_2$ evolution; dashed line: amount of generated H$_2$.

H$_2$ formation started immediately upon light irradiation of these solutions and their rates increased sharply, reaching a maximum for WRC concentrations of 1 μM after about 1 h. The rate then decreased steadily until H$_2$ formation ceased after about 70 h (Figure 7).

Complexes **2a**–**4a** achieved turnover numbers (TONs, H$_2$/Co) up to 17'200 ± 1'800 for **2a**, 13'800 ± 1'500 for **3a** and 21'900 ± 1'200 for **4a** at 1 μM (Figure 8). The increase in TONs at low concentrations implies that overall performance is not limited by the stability of the WRCs. The maximal turnover frequencies (TOF_{max}, H$_2$/WRC/h) steadily increased throughout the concentration range and consequently, the maximal rates of H$_2$ production remain quite constant (Figure 9 and ESI Table S1, nmol/s). The rate of H$_2$ formation is therefore limited by the PS cycle, even at 1 μM WRC and 500 μM PS. Both, the high TONs and TOFs, corroborate the excellent performance of the presented WRCs, which compare well with a previously reported Co^{II} complex of a pentadentate polypyridyl ligand (TOF_{max} 5880 ± 360, TONs of 33'300 ± 1500).[45] Although insoluble, suspensions of **1a** in water (total "concentration" of 175 μM) showed constant H$_2$ production over more than 5 d. However, since the conditions were not homogeneous, **1a** was not included in this study. The PS $[Ru(bpy)_3]^{2+}$ was not detectable anymore at the end of all catalyses. Addition of an equal amount of fresh PS into a sample of **4a** (5 μM) re-established H$_2$ evolution. The 2nd cycle gave another 23 % of the initially formed H$_2$, showing that the WRC was still present (ESI, Figure S14). At high WRC concentrations, catalysis ceased since all sacrificial electron donor (TCEP) was consumed and converted into its oxidised form (^{31}P NMR). The bromide-free complexes **2b**–**4b** showed comparable TOFs and TONs as **2a**–**4a**, in line with complete Br$^-$ dissociation in H$_2$O (ESI, Table S1). Blank experiments at identical photon flux, with NaHasc/TCEP and PS but without WRC, gave 4 μmol of H$_2$ (1.6 TON in Ru, H/Ru). Irradiation experiments with NaHasc/TCEP and **3a** but without PS yielded no H$_2$ at all and catalysis with $CoBr_2$ instead of **2a-4a** gave only marginal amounts of H$_2$ in the presence of PS and NaHasc/TCEP due to PS decomposition. A Hg poisoning experiment with **2a** and **4a** at 5 μM showed the same H$_2$ evolution course as without Hg, confirming that colloids were not involved in catalysis.

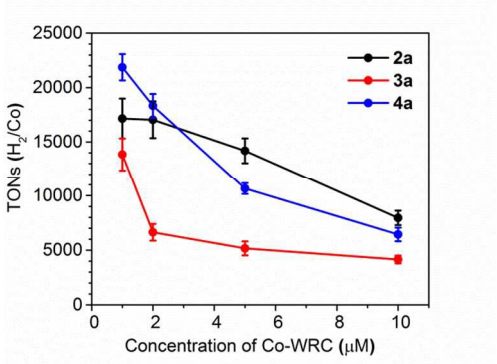

Fig. 8 WRC-concentration dependency study of turnover numbers in cobalt (H$_2$/Co) for catalysts **2a**, **3a** and **4a**. Conditions: Total volume

10 mL, H_2O, 500 μM $[Ru(bpy)_3]Cl_2$, 0.1 M TCEP, 0.1 M NaHasc, pH 5, 453 nm LED, photon flux of 0.30 ± 0.02 μE/s.

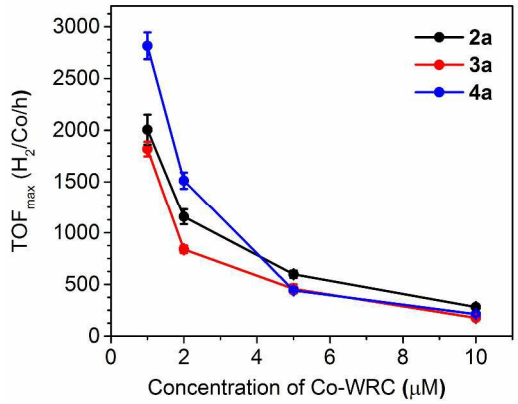

Fig. 9 WRC-concentration dependency study of turnover frequency in cobalt (H_2/Co/h) for catalysts **2a**, **3a** and **4a**. Conditions: Total volume 10 mL, H_2O, 500 μM $[Ru(bpy)_3]Cl_2$, 0.1 M TCEP, 0.1 M NaHasc, pH 5, 453 nm LED, photon flux of 0.30 ± 0.02 μE/s.

Conclusions

In extension to the well studied cobalt complexes of acyclic polypyridyl ligands, we introduced macrocyclic, bis-bipyridyl chelators, reminiscent in their basic structures to porphyrins. Much less investigated than the latter ligands, macrocyclic bis-bipyridyl ligands offer a very stable scaffold for cobalt and probably also for other 3d cations of interest for catalytic processes. We exemplified the catalytic activities with a series of alkylated macrocyclic bis-bipyridyl Co^{II} complexes, featuring comparable performance for catalytic H_2 formation as their acyclic counterparts, and clearly exceeding non-pyridyl based cobalt WRCs. The basic pyrphyrin framework furthermore allows for a straight introduction of (functional) side chains. The presented alkyl groups do not only improve solubility but they also influence the electronics on the metal centre as shown with electrochemical data. In conclusion, Co^{II} complexes with macrocyclic bis-bipyridyl ligands offer manifold opportunities in their basic structure for rationally designing future WRC's with enhanced H_2 producing properties.

Acknowledgements

Financial Support from the University of Zurich, the University Research Priority Program (URPP) ''Light to chemical energy conversion'' (LightChEC) and the Swiss National Science Foundation Sinergia project, CRSII2-136205/1 are gratefully acknowledged.

Notes and references

[a] Department of Chemistry, University of Zurich, Winterthurerstr. 190, CH-8057 Zurich, Switzerland. E-mail: ariel@chem.uzh.ch

[b] Institute of Physics, University of Zurich, Winterthurerstr. 190, CH-8057 Zurich Switzerland

[c] The authors contributed equally to this work.

† Electronic Supplementary Information (ESI) available: Methods, Syntheses, Crystal Data, Calculations, SQUID Measurements, Bromide Dissociation in H_2O, Electrochemistry in H_2O, Stability in H_2O and Photocatalysis. See DOI: 10.1039/b000000x/

1 O. Morton, *Nature*, 2006, **443**, 19-22.
2 F. Gloaguen and T. B. Rauchfuss, *Chem. Soc. Rev.*, 2009, **38**, 100 108.
3 S. Losse, J. G. Vos and S. Rau, *Coord. Chem. Rev.*, 2010, **254**, 2492-2504.
4 V. Artero, M. Chavarot-Kerlidou and M. Fontecave, *Angew. Chem. Int. Ed.*, 2011, **50**, 7238-7266.
5 W. T. Eckenhoff and R. Eisenberg, *Dalton Trans.*, 2012, **41**, 13004-13021.
6 J. L. Dempsey, B. S. Brunschwig, J. R. Winkler and H. B. Gray, *Acc. Chem. Res.*, 2009, **42**, 1995-2004.
7 Z. Han, L. Shen, W. W. Brennessel, P. L. Holland and R. Eisenberg, *J. Am. Chem. Soc.*, 2013, **135**, 14659-14669.
8 H. I. Karunadasa, C. J. Chang and J. R. Long, *Nature*, 2010, **464**, 1329-1333.
9 J. P. Bigi, T. E. Hanna, W. H. Harman, A. Chang and C. J. Chang, *Chem. Commun.*, 2010, **46**, 958-960.
10 Y. Sun, J. P. Bigi, N. A. Piro, M. L. Tang, J. R. Long and C. J. Chang, *J. Am. Chem. Soc.*, 2011, **133**, 9212-9215.
11 L. Tong, R. Zong and R. P. Thummel, *J. Am. Chem. Soc.*, 2014, **136**, 4881-4884.
12 M. Guttentag, A. Rodenberg, C. Bachmann, A. Senn, P. Hamm and R. Alberto, *Dalton Trans.*, 2013, **42**, 334-337.
13 C. Bachmann, M. Guttentag, B. Spingler and R. Alberto, *Inorg. Chem.*, 2013, **52**, 6055-6061.
14 T. Nakazono, A. R. Parent and K. Sakai, *Chem. Commun.*, 2013, **49**, 6325-6327.
15 M. Natali, A. Luisa, E. Iengo and F. Scandola, *Chem. Commun.*, 2014, **50**, 1842-1844.
16 M. Isaacs, J. C. Canales, M. J. Aguirre, G. Estiú, F. Caruso, G. Ferraudi and J. Costamagna, *Inorg. Chim. Acta*, 2002, **339**, 224-232.
17 J. Canales, J. Ramirez, G. Estiu and J. Costamagna, *Polyhedron*, 2000, **19**, 2373-2381.
18 S. Ogawa, R. Narushima and Y. Arai, *J. Am. Chem. Soc.*, 1984, **106**, 5760-5762.
19 S. Ogawa, T. Uchida, T. Uchiya, T. Hirano, M. Saburi and Y. Uchidac, *J. Chem. Soc., Perkin Trans. 1*, 1990, 1649-1653.
20 J. Morita, S. Tsuchiya, N. Yoshida, N. Nakayama, S. Yokokawa and S. Ogawa, *Tetrahedron*, 2007, **63**, 9522-9530.
21 S. Tsuchiya, Y. Nakatani, R. Ibrahim and S. Ogawa, *J. Am. Chem. Soc.*, 2002, **124**, 4936-4937.
22 Z. Zhu, K. Takano, A. Furuhama, S. Ogawa and S. Tsuchiya, *Bull. Chem. Soc. Jpn.*, 2007, **80**, 686-693.
23 R. Ibrahim, S. Tsuchiya and S. Ogawa, *J. Am. Chem. Soc.*, 2000, **122**, 12174-12185.
24 S. Ogawa and S. Shiraishi, *J. Chem. Soc., Perkin Trans. 1*, 1980, 2527-2530.
25 A. Furuhama, K. Takano, S. Ogawa and S. Tsuchiya, *Comp. Theor. Chem.*, 2003, **620**, 49-63.
26 G. Estiu, J. Canales, J. Ramirez and J. Costamagna, *J. Coord. Chem.*, 2001, **54**, 193-214.
27 A. R. De Sànchez, J. R. Anacona and V. E. Màrquez, *Supramol. Chem.*, 1994, **4**, 9-12.
28 H. Endres and M. Hunziker, *J. Cryst. Mol. Struct.*, 1979, **9**, 77-85.
29 W.-J. Wang, A. Sengul, C.-F. Luo, H.-C. Kao and Y.-H. Cheng, *Tetrahedron Lett.*, 2003, **44**, 7099-7101.
30 P. Kumar, R. S. Madyal, U. Joshi and V. G. Gaikar, *Ind. Eng. Chem. Res.*, 2011, **50**, 8195-8203.

31 G. R. Newkome, Y. J. Joo and F. R. Fronczek, *J. Chem. Soc., Chem. Commun.*, 1987, 854-856.
32 B. Spingler, S. Schnidrig, T. Todorova and F. Wild, *CrystEngComm*, 2012, **14**, 751-757.
33 L. J. Farrugia, in *ORTEP-3 for Windows – a version of ORTEP-III with a Graphical User Interface (GUI)*, 1997.
34 S. S. Batsanov, *Inorg. Mater.*, 2001, **37**, 871-885.
35 B. Wu, D. Yuan, B. Lou, L. Han, C. Liu, C. Zhang and M. Hong, *Inorg. Chem.*, 2005, **44**, 9175-9184.
36 D. R. Lide, in *CRC Handbook of Chemistry and Physics*, 95 edn., 2014, vol. 9, 48.
37 K. H. Linke, F. Dürholz and P. Hädicke, *Z. Anorg. Allg. Chem.*, 1968, **356**, 113-117.
38 U. K. Das, J. Bobak, C. Fowler, S. E. Hann, C. F. Petten, L. N. Dawe, A. Decken, F. M. Kerton and C. M. Kozak, *Dalton Trans.*, 2010, **39**, 5462-5477.
39 J. Matsumoto, T. Suzuki, Y. Kajita and H. Masuda, *Dalton Trans.*, 2012, **41**, 4107-4117.
40 Y. Xie and T. W. Hamann, *J. Phys. Chem. Lett.*, 2013, **4**, 328-332.
41 G. N. Schrauzer and L.-P. Lee, *J. Am. Chem. Soc.*, 1968, **90**, 6541-6543.
42 J. P. Collman, J. I. Brauman, K. M. Doxsee, T. R. Halbert, S. E. Hayes and K. S. Suslick, *J. Am. Chem. Soc.*, 1978, **100**, 2761-2766.
43 H. M. M. Hesse, B. Zeeh, *Spektroskopische Methoden in der organischen Chemie*, Thieme, Germany, 8 edn., 2005.
44 J. Wang, *Analytical Electrochemistry*, Wiley-VCH, 3 edn., 2006.
45 C. Bachmann, B. Probst, M. Guttentag and R. Alberto, *Chem. Commun.*, 2014, **50**, 6737-6739.

TOC Entry

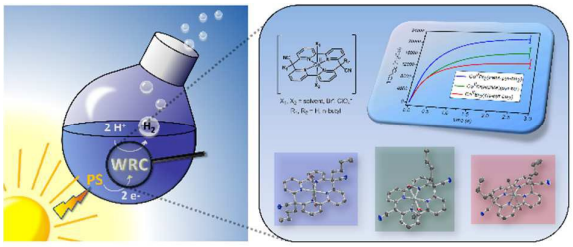

Photocatalytic proton reduction is demonstrated using a new type of cobalt catalysts with macrocyclic bis-bipyridine ligand frameworks, achieving turnover numbers up to 20'000 H2/Co